



## Analysis on the growth of different shapes of mineral microcracks in microwave field

Qin Like

*School of Architecture and Civil Engineering Xi'an University of Science and Technology, Xi'an 710054, P.R China  
422576294@qq.com*

Dai Jun

*School of Architecture and Civil Engineering Xi'an University of Science and Technology, Xi'an 710054, P.R China*

**ABSTRACT.** Microwave heating-assisted ore grinding and crushing can effectively increase the dissociation energy of minerals and decrease energy consumption. Microcrack growth and distribution characteristics inside different shapes of ore particles, which are composed of galena and calcite under microwave irradiation, were analyzed using discrete element method to explore the effects of mineral shapes on microwave-assisted dissociation. Growth laws on the total number of microcracks, numbers of microcracks in galena and calcite, and boundary damage rate against irradiation time under high power and low power were studied. Research results demonstrated that mineral shape mainly affects the quantity of microcracks inside ores but does not their growth law.

**KEYWORDS.** Microwave heating; Ore crushing and grinding; Mesoscale simulation; Microcrack growth; Energy consumption.

### INTRODUCTION

Costs for ore crushing and grinding in dressing plants account for over 40% of the total, and investments for ore crushing and grinding take up for 60% of the total. However, ore crushing and grinding have significantly low energy utilization. Only 1% energy is used for ores to develop new surfaces, and a large amount of energy is lost through heating, noise, and friction [1, 2]. Many improvement methods have been proposed to reduce energy and steel consumptions and increase energy utilization. Among these methods, microwave-assisted technology appears promising [2, 3].

Many gangue minerals in ore (e.g., quartz, calcite, and white mica) are wave transmitting materials, which can be difficult to heat by microwaves. However, unit element ores, most sulfide ores, and oxidized ores (e.g., iron, copper, lead sulfide, pyrite, and manganese oxide ores) absorb materials and can be heated in microwave field for a short time [5-7]. Therefore, significant temperature difference and temperature stress are produced between different minerals under microwave irradiation and induce many cracks in minerals [8, 9].



## STATE OF THE ART

**V**orster et al. [10] ground and floated massive copper sulfide ores in Neves-Corvo Mine after microwave irradiation and found that microwave pre-irradiation can reduce Bond's work index of minerals by 70% and significantly increase the single separation degree of useful minerals after ore grinding. Mamdouh Omran et al. [11] exposed iron ores to microwave irradiation and conducted electron microscopic scanning to ores. Their experiment confirmed that microwave heating resulted in microcracks developing easily between minerals and gangue compared with the traditional heating method. Guo Shenghui [12] and R.K. Amankwah et al. [13] exposed ilmenite and gold ores to microwave irradiation and discovered that microwave irradiation induced microcracks between useful minerals and gangue. These microcracks can effectively facilitate the separation of minerals and gangue. The tests showed that microwave irradiation can enhance the dissociation ability of minerals, and that microcracks in minerals are the root source of mineral dissociation capability.

Determining temperature, stress, and strain distributions in minerals under microwave irradiation through tests can be difficult. Thus, the numerical approach has become the main method used in this field. Huijun Cui et al. [14] simulated the temperature rise curve of carbon-chromium powder using the finite element method (FEM). Qin Like et al. [15] studied temperature distribution in ore particles and its influencing factors. D.A.Jones [16] analyzed temperature-stress distribution in ore particles composed of pyrite and calcite and corresponding damages based on finite difference. A.Y. Ali [17] and Qin Like et al. [18, 19] examined the damages of galena-calcite boundaries in a microwave field based on the finite difference method and explored the corresponding influencing factors. Yicai Wang [20] and Qin Like et al. [21] investigated temperature and stress distribution characteristics in monocrystal minerals using FEM. Ge Wang [22] and A.Y. Ali et al. [23] discussed the distribution characteristics of microcracks in minerals using the discrete element method (DEM).

Interesting findings concerning microwave-assisted ore grinding and crushing have been obtained. However, the influence mechanism of mineral shape on microcrack distribution and development inside ores under microwave irradiation remains unknown. Therefore, the effects of mineral shapes on microcrack distribution and the different factors of ore particles composed of galena and calcite under microwave irradiation were studied from the mesoscopic perspective by using particle flow code (PFC) a commercial Discrete Element Method software from Itasca [24].

## METHODOLOGY

### *Computing method*

**T**he energy balance equation can be expressed as follows:

$$-\frac{\partial q_i}{\partial x_i} + q_v = \rho C \frac{\partial T}{\partial t} \quad (1)$$

where

- $q_i$  is the heat flux vector ( $\text{W}/\text{m}^3$ ) that can be calculated using Fourier's law,
- $x_i$  refers to the position coordinates,
- $q_v$  is the amount of heat generated under microwave irradiation ( $\text{W}/\text{m}^3$ ),
- $\rho$  refers to material density ( $\text{kg}/\text{m}^3$ ),
- $C$  is the specific heat capacity of the material ( $\text{J}/\text{kg} \text{ }^\circ\text{C}$ ),
- $q_v$  is equal to  $P_d$ .

The heat quantity generated by an object under microwave irradiation is determined mainly by microwave frequency and electric field intensity. The amount of heat generated by an object per unit volume can be calculated using Eq. (2).

$$P_d = 2\pi f \epsilon_o \epsilon_r'' E_o^2 \quad (2)$$

where

$P_d$  is the power density of the microwave ( $\text{W}/\text{m}^3$ ), which refers to the power required for the microwave to transform into heat energy,

$f$  is the diffusion frequency of the microwave (Hz),



$\epsilon_0$  is the vacuum dielectric coefficient ( $8.854 \times 10^{-12}$  F/m),

$\epsilon''_r$  is the dielectric dissipation loss factor of the medium,

$E_0$  refers to the effective value of the electric field (V/m).

When exposed to microwave irradiation, calcite absorbs a small amount of microwave energy. During calculation, calcite is assumed not to generate heat [25].

The strain caused by the temperature change in PFC is expressed by the radius change of disks:

$$\Delta R = \alpha R \Delta T \quad (3)$$

where

$\Delta R$  is the radius change of disks,

$\alpha$  is the coefficient of the linear thermal expansion associated with the disk (1/ °C),

R represents the disk radius,

$\Delta T$  is the temperature change.

The normal component of the bond force caused by the temperature range in a parallel-bonded material is

$$\Delta F^n = \bar{k}_n A (\bar{\alpha} L \Delta T) \quad (4)$$

where

$\Delta F^n$  is the normal connection force of disks,

$\bar{k}_n$  is the bond normal stiffness (Pa),

A is the area of the bond cross section,

$\bar{\alpha}$  is the expansion coefficient of the bond material,

L is the bond length.

In a parallel bond model, the generated microcracks are divided into tensile and shear as shown in Fig. 1 [26]. When the tensile bonding force is greater than the bonding strength, tensile microcracks will be generated; when the shear bonding force is greater than the shear bonding strength, shear microcracks will be generated.

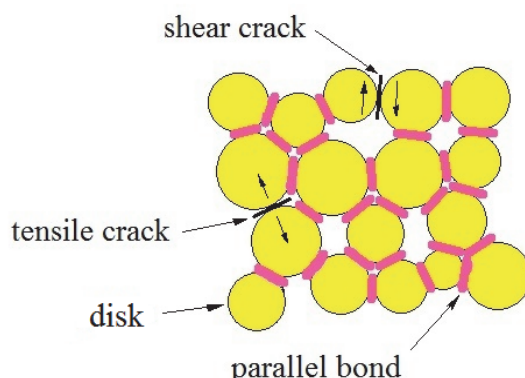
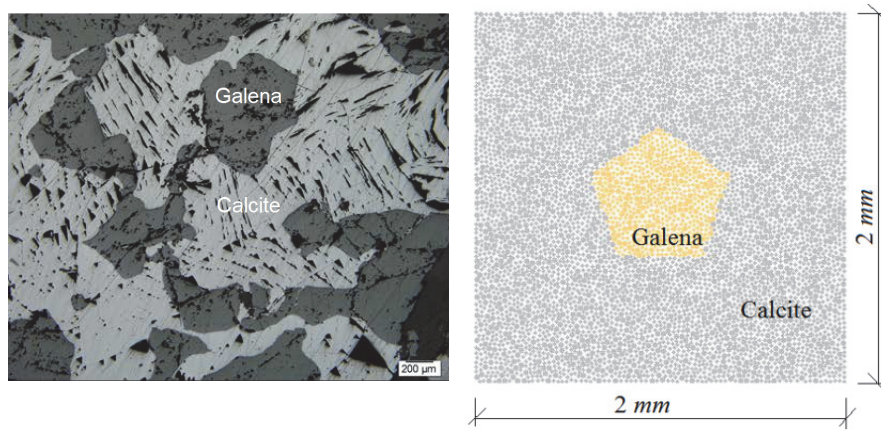


Figure 1: Illustration of bonded-particle models and meso-mechanical behavior

### Calculation Model

The mineral particle model, which is composed of galena and calcite, is shown in Fig. 2. The model is square with galena in the center and calcite surrounding it. The model measures 2 mm×2 mm, and galena is 0.36 mm<sup>2</sup> (i.e., regular triangle, square, regular pentagon, and round in this paper), which accounts for 9% of the mineral particle. The initial temperature of the model was set at 25 °C. Only galena absorbs microwave energy when exposed to microwave irradiation. Minimal heat exchange is observed between the mineral and surrounding environment because of the short microwave irradiation. Therefore, the model boundaries have heat insulation. The model boundary is free of any constraint.



(a) SEM image of galena ore      (b) computed model of ore  
Figure 2: Geometric plot of computed model.

Density ( $\rho$ ), elasticity modulus (E), Poisson's ratio ( $\mu$ ), and tensile strength (T) of galena and calcite are listed in Tab. 1 [27, 28].

	$\rho$ (kg/m <sup>3</sup> )	E (GPa)	$\mu$	T (MPa)
Calcite	2712	83.8	0.31	12
Galena	5016	272	0.16	12

Table 1 Mechanical properties of the discs

The PFC model parameters include minimum disk radius  $R_{\min}=0.02$  mm, disk size ratio  $R_{\max}/R_{\min}=1.66$ , and the total number of disks (6046). The other parameters that define a parallel-bonded material in PFC include solid density  $\rho_b$ , Young's modulus at each particle-particle contact  $E_c$ , ratio of particle normal to shear stiffness  $k_n/k_s$ , particle friction coefficient  $\mu$ , radius multiplier used to set the parallel-bond radii  $\bar{\lambda}$ , Young's modulus of each parallel-bond  $\bar{E}_c$ , ratio of parallel-bond normal to shear stiffness  $\bar{k}_n / \bar{k}_s$ , normal strength of the cement  $\bar{\sigma}_c$ , and shear strength of the cement  $\bar{\tau}_c$ . The biaxial and Brazilian tests were employed for parameter calibration (Tabs. 2 and 3).

	$\rho_b$ (kg/m <sup>3</sup> )	$E_c$ (GPa)	$k_n/k_s$	$U$
Calcite	3228.6	91	5	0.5
Galena	9044	73	3	0.5

Table 2: Mechanical properties of the discs.

	$\bar{\lambda}$	$\bar{E}_c$ (GPa)	$\bar{k}_n / \bar{k}_s$	$\bar{\sigma}_c = \bar{\tau}_c$ (MPa)
Calcite	1	91	5	49±10
Galena	1	73	3	49±10

Table 3: Mechanical properties of the cement.

The thermal conductivity and specific heat capacity of galena and calcite are shown in Tab. 4, while their thermal expansion coefficients are presented in Tab. 5 [27, 28].



	Thermal conductivity (w/m)			Specific heat capacity (J/kg °C)		
	25 °C	100 °C	227°C	25 °C	227 °C	727 °C
Calcite	4.02	3.01	2.55	819	1051	1238
Galena	2.76	2.45	1.92	208	215	234

Table 4: Thermal conductivity and specific heat capacity in different temperatures.

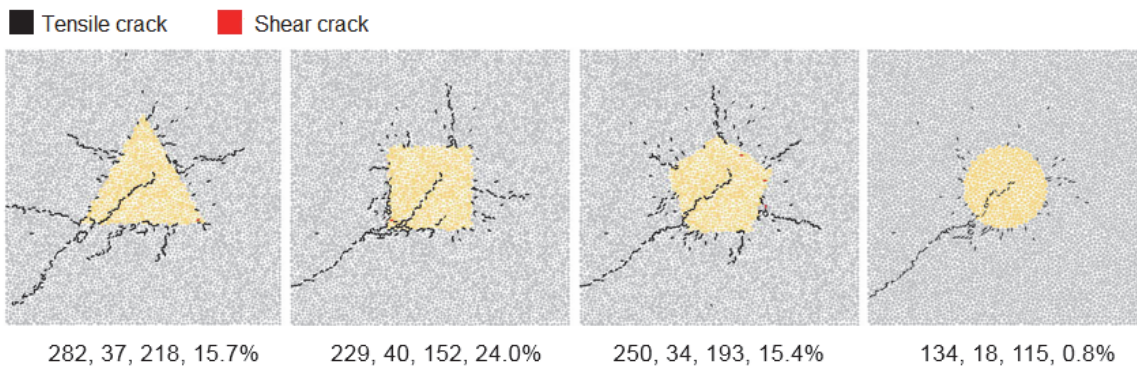
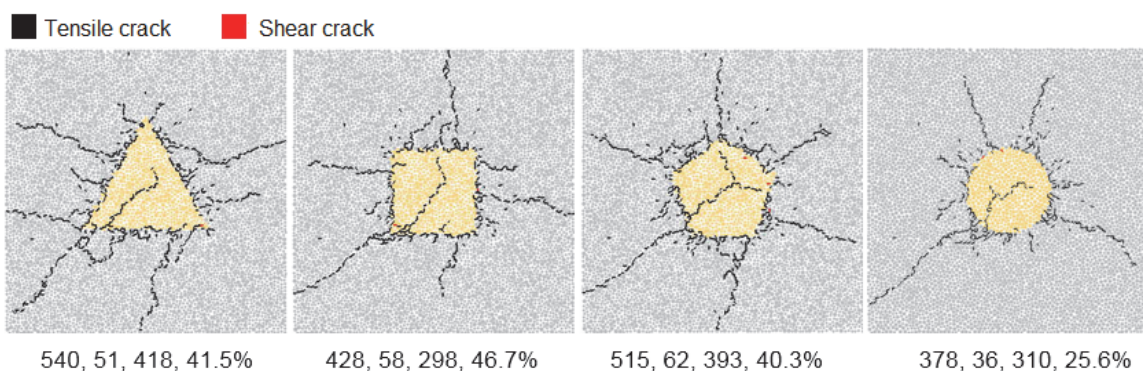
	100 °C	200 °C	400 °C	600 °C
Calcite	1.31	1.58	2.01	2.4
Galena	6.12	6.10	6.32	--

Table 5 :Thermal expansion coefficient in different temperatures ( $10^{-5}$ ).

## CALCULATION RESULTS AND ANALYSIS

### Analysis under low power density

**M**icrocrack distributions under different irradiation times (0.5 and 1.5 s) when  $P_d=1\times 10^9\text{W/m}^3$  are shown in Figs. 3 and 4. The total number of microcracks, number of microcracks in galena, number of microcracks in quartz, and boundary damage rate are given. Viewed as stress types, different shapes of minerals develop many tensile cracks and few shear cracks. The shape of galena will not influence crack types. Cracks can be divided into three types according to position distribution: 1) Diffused cracks, which develop in calcite and point to the center, which can break gangue. 2) Calcite-galena interface cracks, which can separate galena from calcite. 3) Cracks in galena, which are extensions of the first crack in calcite into galena during early irradiation. The first two types are good for mineral dissociation while the third type breaks minerals. Excessive cracks in galena are disadvantageous for mineral dissociation.

Figure 3: Microcrack distributions in different shapes of minerals ( $t = 0.5$  s)Figure 4: Relation curves of microcrack number and irradiation time ( $t = 1.5$  s)

Relations between the total number of microcracks and number of microcracks in calcite and irradiation time under different shapes of galena are presented in Figs. 5 and 6. The relation curve between boundary damage rate of minerals and irradiation time is presented in Figs. 7. Galena shape is insignificant to the growth law of the total number of microcracks and the number of microcracks in calcite against time. The total number of microcracks in ore and the number of microcracks in calcite increase as irradiation continues. The growth rate of curves decreases with the increase of irradiation time. The shape of the galena affects the number of cracks. Fig. 5 shows that at different irradiation times, the ore with triangle galena had the highest total number of microcracks, followed by pentagonal, quadrilateral, and circular galena. Fig. 6 shows that calcite has the highest number of microcracks at different irradiation times, followed by pentagon galena. The number of microcracks in the quadrilateral galena is higher than that in the circular galena in the first 2.8 s irradiation but the opposite occurs when irradiation time exceeds 2.8 s.

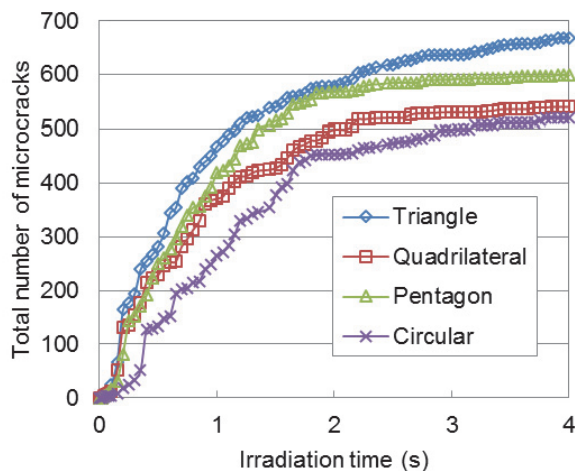


Figure 5: Relation curve between the total number of microcracks and irradiation time.

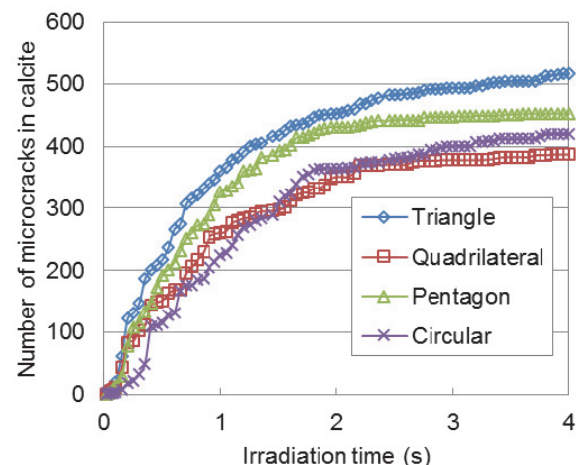


Figure 6: Relation curve between number of microcracks in calcite and irradiation time.

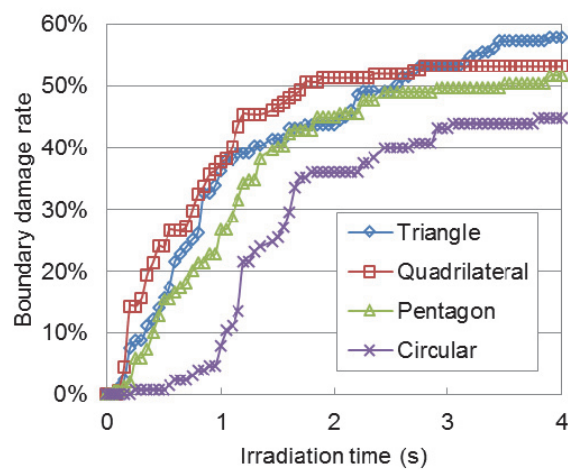


Figure 7: Relation curve between boundary damage rate of minerals and irradiation time

The relationship between the numbers of microcracks in different shapes of galena and irradiation time is shown in Fig. 8. Microcrack growth curve in different shapes of galena can be divided into three stages. For example, in the square galena, the first stage is the sudden increase stage (0.15–0.2 s) when number of microcracks in galena increases quickly and the curve is approximately vertical. The second stage is the linear growth stage (0.2–1.8 s). In the third stage, the number of microcracks in galena (1.8–4.0 s) is stable and the curve is horizontal. Galena shape will not affect microcrack growth stages in galena but can affect the number of microcracks. At different irradiation times, the numbers of microcracks in quadrilateral and pentagonal galena are similar and the highest, followed by the triangular galena and the circular galena.

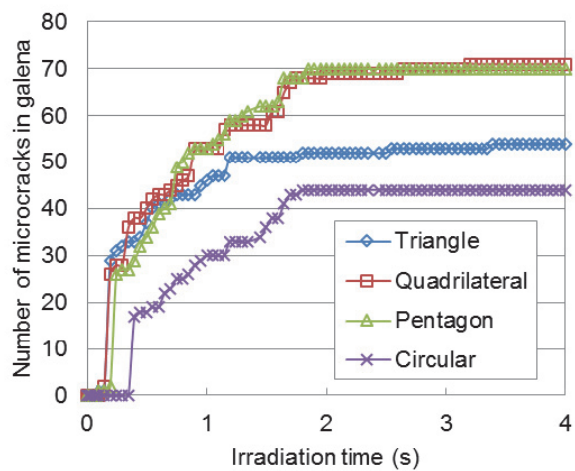
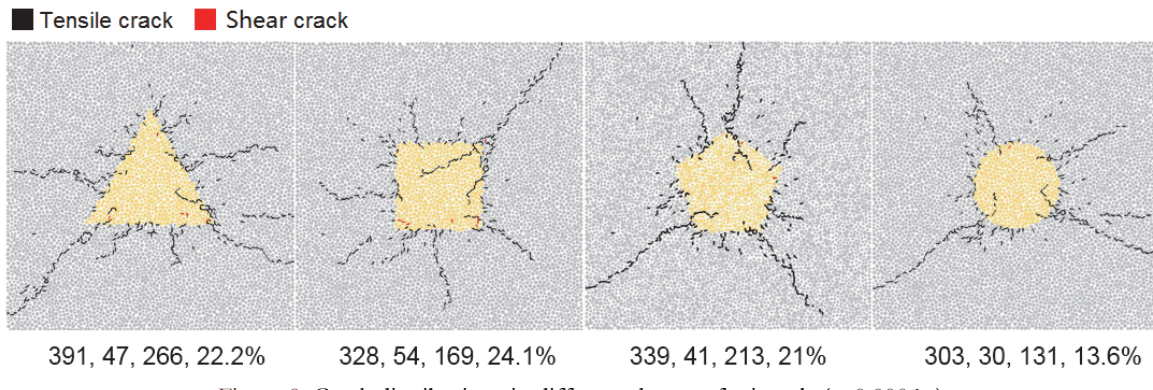
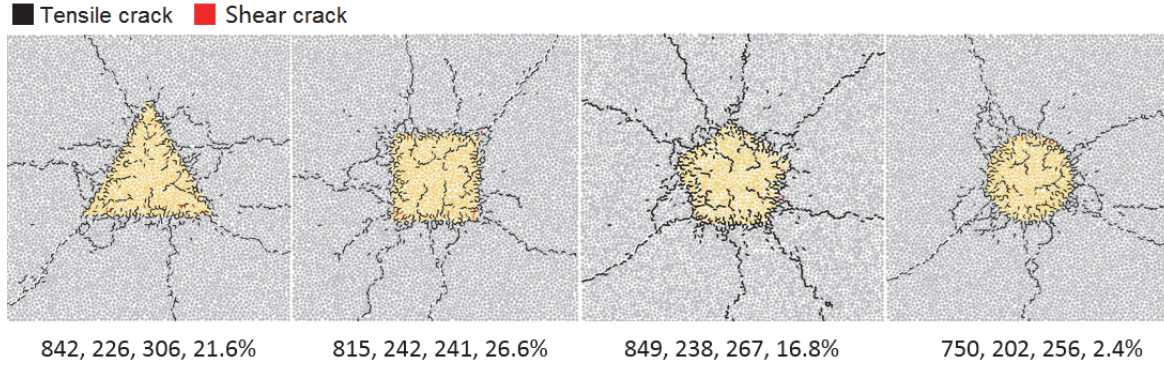


Figure 8: Relation curve between number of microcracks in galena and irradiation time.

#### Analysis under high power density

Crack distributions under different irradiation times (0.0006 and 0.006 s) when  $P_d=1\times10^{11}\text{W/m}^3$  are shown in Figs. 9 and 10. The total number of microcracks, number of microcracks in galena, number of microcracks in quartz, and boundary damage rate are presented. Figs. 9 and 10 show that microcracks under high-power microwave irradiation are mainly tensile cracks.

Figure 9: Crack distributions in different shapes of minerals ( $t=0.0006$  s).Figure 10: Crack distributions in different shapes of minerals ( $t=0.006$  s).

The relation curves between the total number of microcracks and the number of microcracks in galena and irradiation time under different shapes of galena are presented in Figs. 11 and 12. Microcrack growth has a similar law under different shapes of galena. The total number of microcracks and number of microcracks in galena are positively correlated with irradiation time, whereas microcrack growth rate is negatively correlated. The numbers of microcracks in different shapes

of galena at different irradiation times are similar; however, the number of microcracks in circular galena is smaller after 0.004 s.

The relation curves between the number of microcracks in calcite and boundary damage rate and irradiation time under different shapes of galena are shown in Figs. 13 and 14. The growth of boundary damage rate and the number of microcracks in calcite can be divided into two stages. The first stage is from 0 s to 0.0035 s when the number of cracks in calcite increases quickly (ranging 490–512), and the boundary damage rate varies within 51%–55%. This rapid increase reflects the insignificance of galena shape. The second stage starts from 0.0035 s when the number of microcracks in calcite remains the same, indicating that the microcracks in minerals after 0.0035 s occur mainly in the galena, causing the useful minerals to become too broken against mineral separation.

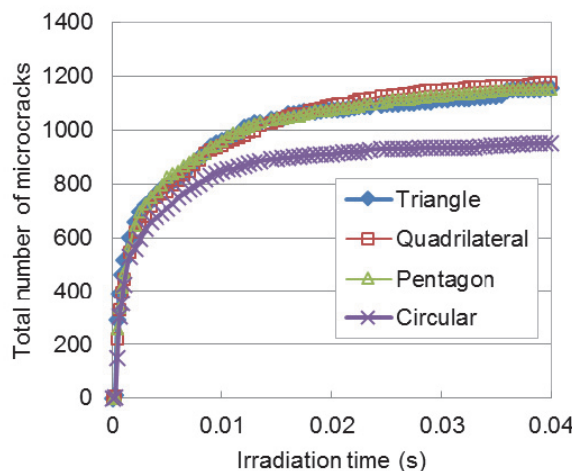


Figure 11: Relation curves between the total number of microcracks and irradiation time.

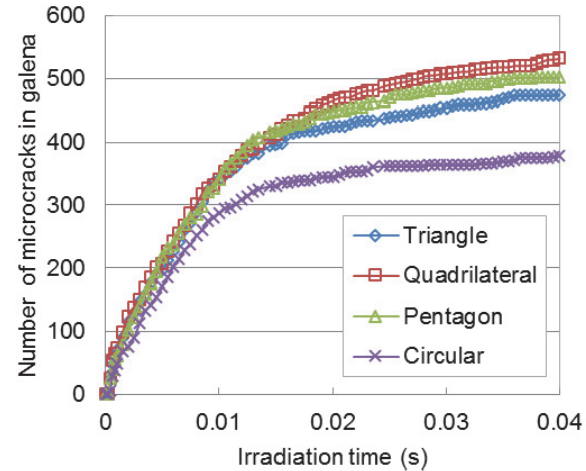


Figure 12: Relation curves between the number of microcracks in galena and irradiation time.

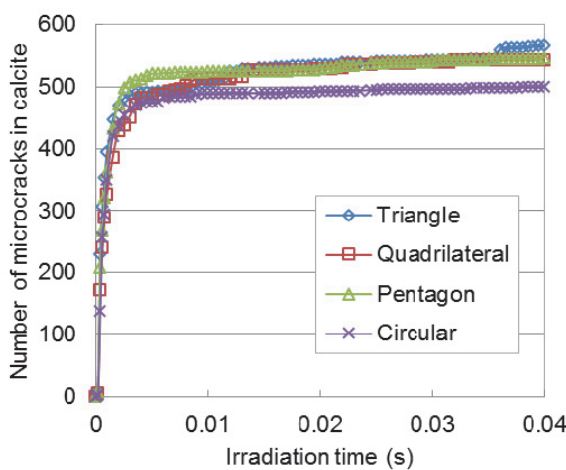


Figure 13: Relation curves between the number of microcracks in calcite and irradiation time.

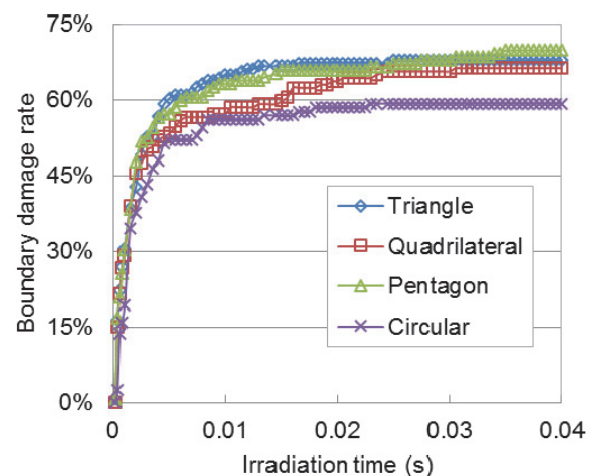


Figure 14: Relation curves between boundary damage rate and irradiation time.

The first stage under high-power microwave irradiation can be used as the optimum irradiation time. The number of microcracks in calcite and boundary damage rate increase quickly within the optimum irradiation time. The total numbers of microcracks are similar for different shapes of galena, indicating that mineral shape will not affect mineral dissociation. However, once irradiation time exceeds the optimum range, microcracks in useful minerals will continue to increase, whereas the number of microcracks in calcite and the boundary damage rate remain the same. Thus, long irradiation time is disadvantageous for mineral dissociation.



## CONCLUSIONS

This paper discusses the crack distribution and development in mineral particles composed of galena and calcite under high and low microwave powers using DEM and a 2D plane strain model. The main conclusions are as follows:

- (1). Microcracks formed in ores are mainly tensile cracks regardless of the level of microwave power and mineral shapes, which are accompanied with few shear cracks. Distribution characteristics and positions indicate that microcracks can be divided into diffused cracks in calcite, calcite-galena interface cracks, and cracks in galena. The first two types of cracks represent the root mechanism for microwave-assisted ore crushing and grinding.
- (2). Under low microwave power, the total number of microcracks, number of microcracks in calcite, number of microcracks in galena, and boundary damage rate are positively correlated with irradiation time. However, their growth rates are negatively correlated. At different irradiation times, the number of microcracks in the different shapes of galena differs significantly. Circular galena had the least microcracks.
- (3). Under high microwave power, the number of microcracks in the different shapes of galena display a similar growth law with irradiation time. Microcrack growth curve can be divided into two stages. The first stage achieves a higher growth rate than the second one. The numbers of microcracks in different shapes of galena are similar at different irradiation time in the first stage. However, the number of microcracks in the circular galena is significantly smaller than those in other shapes of minerals.
- (4). This study suggests the use of high-powered microwave for mineral dissociation and the first growth stage of boundary damage rate as the optimum irradiation time. The numbers of microcracks in different shapes of minerals and their variation laws are basically the same within this optimum irradiation time. The number of cracks in gangue and the boundary damage rate remains unchanged after exceeding the optimum irradiation time.

## ACKNOWLEDGEMENTS

This work was supported by the Foundation of Shaanxi Educational Committee (15JK1471), the China Postdoctoral Science Foundation (2015M572580), and the National Natural Science Foundation of China (No. 51174159).

## REFERENCES

- [1] Qinhuan, J., *Microwave chemistry*. Science Press, Beijing, (1990) 214-216.
- [2] Lubikowski, K., Seebeck phenomenon, calculation method comparison. *Journal of Power Technologies*, 95(1) (2015) 63-67.
- [3] Islam, M. M., Design of a microstrip antenna on duroid 5870 substrate material for ku and k-band applications. *Tehnicki Vjesnik*, 6(2) (2013) 71-77.
- [4] Kolarz, C., Korol, K. B. et al., Model of eco-efficiency assessment of mining production processes. *Archives of Mining Sciences*, 1(2) (2015) 477-482.
- [5] Ghazala, Y., Almas, H., Saira, I., Pollutants generated from pharmaceutical processes and microwave assisted synthesis as possible solution for their reduction - A mini review. *Nature Environment and Pollution Technology*, 11(1) (2012) 29-36.
- [6] Kingman, S. W., Vorster, W., Rowson, N. A., The influence of mineralogy on microwave assisted grinding. *Minerals engineering*, 22 (1) (2015) 160-163.
- [7] Liu, Q., Xiong, Y., Research on application mechanism of microwave in iron ores selective grounding. *Yunnan Metallurgy*, 6 (3) (1997) 25-28.
- [8] Kingman, S.W., Rowson, N.A., Microwave treatment of minerals- a review. *Minerals Engineering*, 11(11) (1998) 1081-1087.
- [9] Kingman, S. W., Jackson, K., Recent developments in microwave assisted combination. *International Journal of Mineral Processing*, 74 (2004) 71-83.
- [10] Vorster, W., Rowson, N. A., Kingman, S. W., The effect of microwave radiation upon the processing of Neves-Corvo copper ore. *International journal of mineral processing*, 63( 3) (2001) 29-44.



- [11] Omran, M., Fabritius, T., Mattila, R., Thermally assisted liberation of high phosphorus oolitic iron ore: A comparison between microwave and conventional furnaces. Powder Technology, 269 (269) (2015) 7-14.
- [12] Sheng-hui, G., Guo, C., Jin-hui, P., et al. Microwave assisted grinding of ilmenite ore. Transactions of Nonferrous Metals Society of China, 21 (9) (2011) 2122-2126.
- [13] Amankwah, R.K., Ofori-Sarpong, G., Microwave heating of gold ores for enhanced grindability and cyanide amenability, Minerals Engineering, 24(6) (2011) 541-544.
- [14] Cui, H., Chen, J., Feng, X., Li, N., Numerical simulation for temperature rising curve of carbon-bearing chromium powder in microwave field. China Metallurgy, 17 (1) (2007) 30-35.
- [15] Like, Q., Jun, D., Temperature distribution and influential factors of ore particle under microwave irradiation. Mining and Metallurgical Engineering, 35(3) (2015) 96-98.
- [16] Jones, D.A., Kingman, S.W., Whittles, D.N., Understanding microwave assisted breakage. Minerals Engineering, 18(7) (2005) 659-669.
- [17] Ali, A.Y., Bradshaw, S.M., Quantifying damage around grain boundaries in microwave treated ores. Chemical Engineering and Processing, 48(11) (2009) 1566-1573.
- [18] Like, Q., Jun, D., Meso-mechanics Simulation Analysis of Microwave-assisted Mineral Liberation. *Frattura ed Integrità Strutturale*, 34 (34) (2015) 543-553.
- [19] Like, Q., Jun, D., Pengfei, T., Study on the Effect of Microwave Irradiation on Rock Strength. Journal of Engineering Science and Technology Review, 8 (4) (2015) 91-96.
- [20] Wang, Y., Djordjevic, N., Thermal stress FEM analysis of rock with microwave energy. International Journal of Mineral Processing, 130(28) (2014) 74-81.
- [21] Like, Q., Jun, D., Juntian, Z., Evolution of temperature and stress in rock under microwave irradiation. Electronic Journal of Geotechnical Engineering, 20(28) (2015) 13507-13516.
- [22] Wang, G., Radziszewski, P., Ouellet, J., Particle modeling simulation of thermal effects on ore breakage. Computational Materials Science, 43(4) (2008) 892-901.
- [23] Ali, A.Y., Bradshaw, S.M., Bonded-particle modelling of microwave-induced damage in ore particles. Minerals Engineering, 23 (10) (2010) 780-790.
- [24] Cundall, P. A., Strack, O. D. L., A discrete numerical model for granular assemblies. Géotechnique, 29(1) (1979) 47-65.
- [25] Chen, T.T., Dutrizac, J.E., Hague, K.E., et al. The relative transparency of minerals to microwave radiation. Canadian Metallurgical Quarterly, 23 (3) (1984) 349-354.
- [26] Potyondy, D.O., Cundall, P.A., A bonded-particle model for rock. International Journal of Rock Mechanics & Mining Sciences, 41(8) (2004), 1329-1364.
- [27] Touloukian, Y. S., Judd, W.R., Physical properties of rocks and minerals, McGraw-Hill Book Company, New York, (1980) 56-63.
- [28] Clark, S. P., Handbook of physical constants. Geological Society of America, New York, (1966) 415-436.